Chinese Chemical Letters 36 (2025) 110195

Contents lists available at ScienceDirect

Chinese Chemical Letters

journal homepage: www.elsevier.com/locate/cclet

Pt/Ti_3C_2 electrode material used for H_2S sensor with low detection limit and high stability

Huakang Zong[a,b], Xinyue Li[b], Yanlin Zhang[c], Faxun Wang[c], Xingxing Yu[b], Guotao Duan[c,*], Yuanyuan Luo[a,b,*]

[a] University of Science and Technology of China, Hefei 230026, China
[b] Key Laboratory of Materials Physics, Institute of Solid State Physics, HFIPS, Chinese Academy of Sciences, Hefei 230031, China
[c] School of Integrated Circuits, Huazhong University of Science and Technology, Wuhan 430074, China

ARTICLE INFO

Article history:
Received 22 February 2024
Revised 30 May 2024
Accepted 30 June 2024
Available online 1 July 2024

Keywords:
H_2S sensor
Pt/Ti_3C_2
Low detection limit
Long term stability
Density functional theory calculation

ABSTRACT

Traditional Pt/C electrode materials are prone to corrosion and detachment during H_2S detection, leading to a decrease in fuel cell-type sensor performance. Here, a high-performance H_2S sensor based on Pt loaded Ti_3C_2 electrode material with -O/-OH terminal groups was designed and prepared. Experimental tests showed that the Pt/Ti_3C_2 sensor has good sensitivity (0.162 μA/ppm) and a very low detection limit to H_2S (10 ppb). After 90 days of stability testing, the response of the Pt/Ti_3C_2 sensor shows a smaller decrease of 2% compared to that of the Pt/C sensor (22.9%). Meanwhile, the sensor also has high selectivity and repeatability. The density functional theory (DFT) calculation combined with the experiment results revealed that the improved H_2S sensing mechanism is attributed to the fact that the strong interaction between Pt and Ti_3C_2 *via* the Pt-O-Ti bonding can reduce the formation energy of Pt and Ti_3C_2, ultimately prolonging the sensor's service life. Furthermore, the catalytic property of Pt can decrease the adsorption energy and dissociation barrier of H_2S on Pt/Ti_3C_2 surface, greatly enhance the ability to generate protons and effectively transfer charges, realizing good sensitivity and high selectivity of the sensor. The sensor works at room temperature, making it very promising in the field of H_2S detection in future.

Hydrogen sulfide (H_2S) is normally a colorless and flammable acidic gas, as well as a toxic gas with a foul egg odor [1,2]. When mixed with air, it can form an explosive mixture, which can cause combustion and explosions when exposed to open flames and high heat [3]. Low concentrations of H_2S cause harm to the eyes, respiratory system, and central nervous system. Inhaling small amounts of high concentrations of H_2S can be fatal in a short period of time [4-6]. In addition, H_2S can also pose a risk of corrosion and aging to the equipment [7]. At present, the sensors used for H_2S detection mainly include optical sensors [8,9], metal oxide semiconductor sensors [10-16], and electrochemical sensors [17-21]. Among them, optical sensors have high accuracy, but high manufacturing costs and complex operations make them only used in certain applications. Metal oxide semiconductor sensors have received extensive research due to their high sensitivity, low cost, and portability. However, their poor selectivity and high operating temperature urge people to continuously improve the sensor performance to meet further applications. As an electrochemical sensor, the proton exchange membrane (PEM) fuel cell-type gas sensor uses Nafion proton membrane as the solid electrolyte to separate the gas from the anode and cathode. After the gas reaches the anode, the oxidation reaction occurs to produce protons and electrons, which are respectively transferred to the cathode through the proton membrane and the external circuit for the reduction reaction. Finally, the current is collected and gas detection is realized. This sensing feature gives the sensors the advantages such as low power consumption, cheap cost, small size, good linear response, and fast response time, making sensors have great potential for application in H_2S detection [22-27].

Pt/C, as the most commonly used catalyst in PEM fuel cell gas sensors, has excellent catalytic performance [28]. However, the weak bonding between Pt and carbon carrier makes carbon material susceptible to corrosion in the oxidizing environment, ultimately leading to the separation and further aggregation of Pt particles from the carrier. In addition, Pt/C has catalytic effects on multiple gases, resulting in poor selectivity of the sensor [29-32]. These issues will reduce the sensitivity and accuracy of sensors, and lead to their complex calibration. Therefore, there is an urgent

* Corresponding authors.
E-mail addresses: duangt@hust.edu.cn (G. Duan), yyluo@issp.ac.cn (Y. Luo).

https://doi.org/10.1016/j.cclet.2024.110195
1001-8417/

need to develop the materials with stable structure and high conductivity as carriers for Pt.

Transition metal carbide (Ti_3C_2, MXene) has been considered an excellent catalyst carrier due to its excellent metal conductivity, two-dimensional properties, and special chemical stability [33,34]. The unique two-dimensional layered structure can not only provide abundant anchoring space but also have abundant surface chemical properties, which are conducive to the loading of Pt nanoparticles. Moreover, its excellent conductivity and structural stability have a positive influence on promoting the oxidation–reduction reaction (ORR) [35]. Therefore, Ti_3C_2 and its composite with Pt catalyst have attracted increasing attention in recent years. For example, researchers found that the terminal groups on the surface of MXene played an important role in the stability of the material, and Ti_3C_2 with -O/-OH terminal groups had excellent chemical stability [36,37]. Meanwhile, Yeongdae Lee demonstrated that Pt loaded on multi-layer Ti_3C_2 (22L-Ti_3C_2) exhibited higher ORR activity compared to single-layer Ti_3C_2 (1L-Ti_3C_2) or few-layer Ti_3C_2 (4L-Ti_3C_2) [33]. Studies also confirmed that Ti_3C_2 support was more corrosion-resistant than carbon support, making the catalyst more durable during repeated ORR cycles [38]. In addition, Z.Y. Zhang, Y.J. Wang, and C.X. Xu showed through experiments that there were strong metal-support interactions (SMSI) between Pt and Ti_3C_2, and Pt/Ti_3C_2 had significantly higher durability and ORR activity than Pt/C [35,39,40]. The above studies indicate the modified Pt/Ti_3C_2 can become an excellent catalyst material with better performance than Pt/C, and can be used for fuel cell-type sensors to improve their performance.

In this work, a fuel cell-type H_2S gas sensor based on Pt loaded Ti_3C_2 electrode material with -O/-OH terminal groups was designed and prepared. Experiment results combined with density functional theory (DFT) calculations indicated that -O/-OH terminal groups of Ti_3C_2 replace -F/-OH terminal groups, and after Pt is loaded on the surface of Ti_3C_2, it results in the formation of the Pt-O-Ti bonding, enhancing the interaction between Pt and Ti_3C_2, and prolonging the service life of the sensor. And the catalytic activity of Pt can decrease the adsorption energy and dissociation barrier of H_2S on the Pt/Ti_3C_2 surface, realizing good sensitivity and high selectivity of the sensor. Ultimately, the SMSI between Pt and Ti_3C_2 and high catalytic activity of Pt make the H_2S sensing performance of Pt/Ti_3C_2 sensor surpass that of Pt/C sensor.

The Ti_3C_2 was prepared by etching the Al layer in Ti_3AlC_2 with *in-situ* generated hydrofluoric acid. In detail, 2 g Ti_3AlC_2 was slowly added to a mixed solution of HCl (40 mL) and LiF (2 g), and then stirred at 25 °C for 48 h. The obtained product was washed multiple times with deionized water until the upper liquid turned black. The precipitate was collected by centrifugation at 4000 rpm and then vacuum dried. Finally, the prepared Ti_3C_2 powder was annealed at 350 °C in H_2 atmosphere for 30 min.

Next, Pt/Ti_3C_2 materials with different Pt mass fractions were prepared by the $NaBH_4$ reduction method. In detail, 50 mmol/L of H_2PtCl_6 and Ti_3C_2 with a certain proportion were added to the beaker, and then an appropriate amount of $Na_3C_6H_5O_7{\cdot}2H_2O$ was added to suppress agglomeration. Subsequently, 50 mL deionized water was added to the beaker and stirred for 20 min to evenly disperse the solute. After the $NaBH_4$ alkaline solution (pH ≥ 13) was added dropwise to the solution above, the obtained solution was stirred in an 80 °C water bath for 2 h. Finally, the obtained product was subjected to multiple washes and filtration, followed by vacuum drying overnight at 80 °C to obtain Pt/Ti_3C_2 with different Pt load amounts. The catalyst materials with Pt mass fractions of 5 wt%, 10 wt%, 20 wt%, and 30 wt% are called Pt_5/Ti_3C_2, Pt_{10}/Ti_3C_2, Pt_{20}/Ti_3C_2, and Pt_{30}/Ti_3C_2, respectively. And their Pt atomic percentages are calculated to be about 0.903%, 1.908%, 4.292%, and 5.723%, respectively. In this work, Pt/Ti_3C_2 materials without specifying the Pt mass fractions are all Pt_{10}/Ti_3C_2.

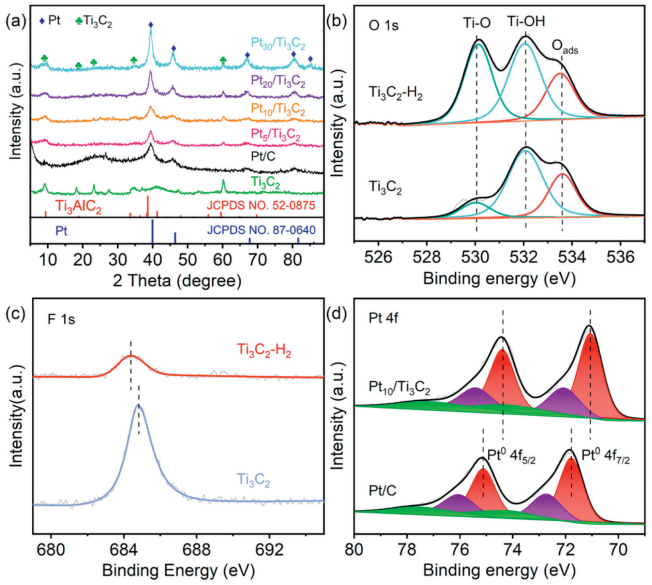

Fig. 1. (a) XRD patterns of six products. XPS spectra of (b) O 1s, (c) F 1s for Ti_3C_2 before and after H_2 annealing, and (d) Pt 4f for Pt/Ti_3C_2 and Pt/C.

The X-ray diffraction (XRD) patterns of Ti_3C_2, Pt/C, and Pt/Ti_3C_2 with different Pt mass fractions are shown in Fig. 1a. Firstly, the diffraction peak of Ti_3AlC_2 at 9.5° (JCPDS No. 52–0875) corresponding to the (002) plane shifts towards a lower angle, while its diffraction peak at 39.0° completely disappears, indicating that Ti_3AlC_2 has successfully transformed into Ti_3C_2 [41,42]. For Pt/Ti_3C_2 and Pt/C, broad diffraction peaks of Pt appear at $2\theta = 40.0°$, 46.4°, 67.9°, 81.6°, and 86.3°. After comparison with the XRD standard card (JCPDS No. 87–0640), it was found that these peaks correspond to the (111), (200), (220), (311), and (222) crystal planes of Pt. These results indicate that Pt was successfully loaded onto the prepared Ti_3C_2. According to the Bragg equation, $n\lambda = 2d\sin\theta$, where n is the diffraction order, λ is the wavelength of the X-ray, θ is the diffraction angle, and d is the interplane spacing, the spacing of the (111) crystal plane of Pt nanoparticles was calculated to be 0.2258 nm. In addition, the intensity of the Pt peak increases with the increase of Pt loading on the surface of Pt/Ti_3C_2.

The XPS spectra of O 1s for Ti_3C_2 after H_2 annealing are shown in Fig. 1b. It was found that the integral area of the Gaussian fitting peak for Ti-OH decreases while that for Ti-O increases, indicating a large amount of -OH terminal groups were converted to -O terminal groups. Fig. 1c shows that compared to before H_2 annealing, the peak intensity of F 1s significantly decreases and its peak position shifts towards lower binding energy after H_2 annealing, indicating a decrease in the -F terminal group. The above result illustrates the terminal groups of Ti_3C_2 converted from -F/-OH to -O/-OH [43,44]. Fig. 1d shows the high-resolution XPS spectra of Pt 4f for Pt/Ti_3C_2 and Pt/C, and there are three bimodal Gaussian fitting peaks of Pt 4f, represented by red, purple, and green peaks corresponding to Pt^0, Pt^{2+}, and Pt^{4+}, respectively. Importantly, there is more Pt^0 in Pt/Ti_3C_2 catalyst than in Pt/C catalyst, which helps to improve the catalytic activity of the material [25]. The binding energy of Pt^0 $4f_{7/2}$ in Pt/C and Pt/Ti_3C_2 catalysts is about 71.80 eV and 71.05 eV, respectively. Compared with Pt/C, the binding energy of Pt 4f for Pt/Ti_3C_2 decreases by about 0.75 eV. This result confirms the presence of SMSI between Ti_3C_2 and Pt, indicating that electrons transfer from Ti_3C_2 to Pt nanoparticles, enhancing the adsorption ability and catalytic activity of Pt/Ti_3C_2 [33], and ultimately improving its sensing performance.

The morphology and structure of the material were further analyzed using field emission scanning electron microscopy (FESEM)

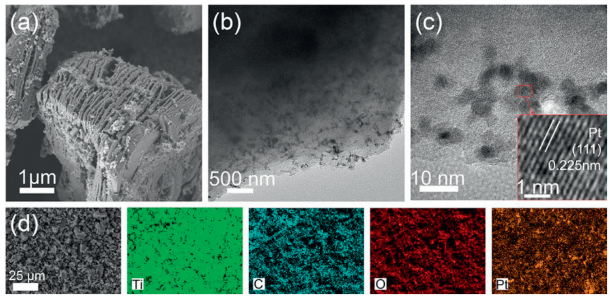

Fig. 2. (a) FESEM image, (b) TEM and (c) HRTEM images of Pt/Ti_3C_2, and (d) FESEM image of Pt/Ti_3C_2 and the corresponding EDS element mapping images of Ti, C, O, and Pt.

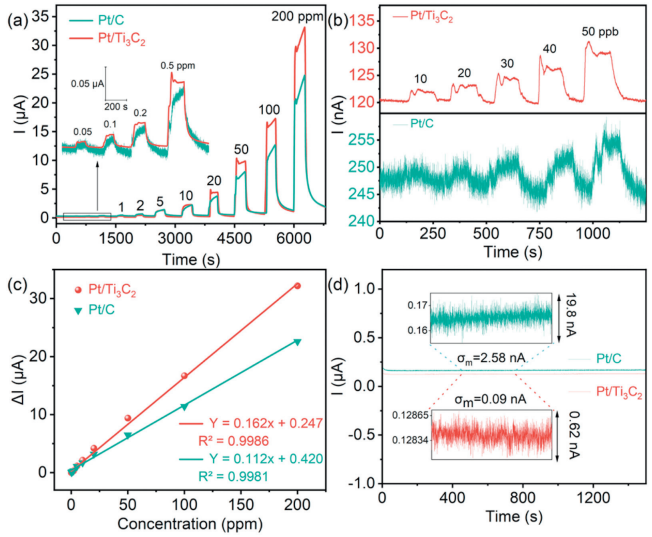

Fig. 3. Response transient curves for the Pt/Ti_3C_2 sensor and the Pt/C sensor exposed to H_2S gas with concentrations ranging from (a) 0.05 ppm to 200 ppm and (b) 10 ppb to 50 ppb. (c) The response values of Pt/Ti_3C_2 and Pt/C based sensors to H_2S concentrations of 0.01 ppb–200 ppm. (d) Current baseline of Pt/Ti_3C_2 and Pt/C sensors in air. The illustration shows an enlarged area of 300 s.

and transmission electron microscope (TEM). Compared with Fig. S2a (Supporting information), the multi-layer structure of the Ti_3C_2 material in Fig. S2b (Supporting information) proves that Ti_3C_2 material was successfully prepared. Fig. S2c (Supporting information) is the FESEM image of commercial Pt/C. It is evident the FESEM and TEM images in Figs. 2a and b both show that many nanoparticles are dispersed on the surface of Ti_3C_2. The lattice spacing of the black particles in Fig. 2c is analyzed to be $d = 0.2252$ nm, corresponding to the (111) crystal plane of Pt. This is also consistent with the results calculated from XRD patterns using the Bragg equation. The energy dispersive spectrometer (EDS) spectrum of Pt_{10}/Ti_3C_2 catalytic material (Fig. 2d) proves the existence of Ti, C, O, and Pt elements. The actual content of Pt in the product was verified through EDS, and the mass fractions of Pt in four products are 3.97 wt%, 9.42 wt%, 19.5 wt%, and 28.3 wt%, respectively, which is consistent with their feed ratio. The mass ratio of Pt in commercial Pt/C is 10.4 wt%.

The gas sensing performances of the Pt/Ti_3C_2 sensor and the Pt/C sensor were first compared. The response time and recovery time of the Pt/Ti_3C_2 sensor and the Pt/C sensor for 50 ppm H_2S are 9 s/43 s and 11 s/42 s, respectively, indicating they have the ability to quickly detect H_2S (Fig. S3 in Supporting information). The dynamic sensing responses of the Pt/Ti_3C_2 sensor and the Pt/C sensor to different concentrations of H_2S ranging from 50 ppb to 200 ppm (Fig. 3a) and 10 ppb to 50 ppb (Fig. 3b) were measured.

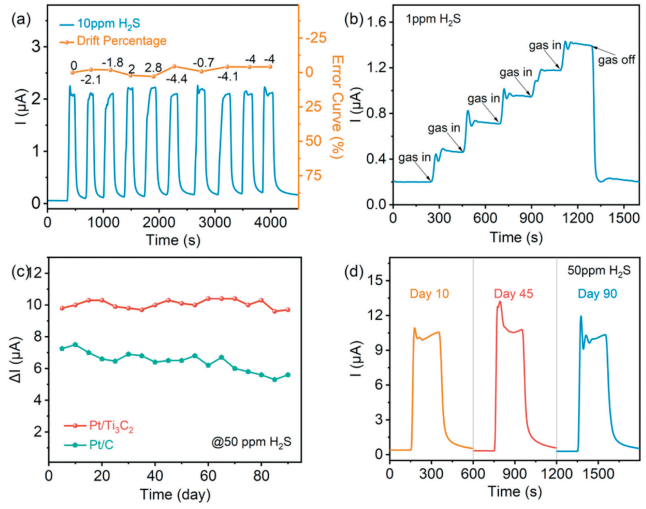

Fig. 4. (a) Ten-cycle repeated response values of Pt/Ti_3C_2 sensor to 10 ppm H_2S. (b) Experimental results of five consecutive injections of 1 ppm H_2S without recovery. (c) Long-term stability of Pt/Ti_3C_2 sensor and Pt/C sensor. (d) Response/recovery curves of Pt/Ti_3C_2 sensor on the 10th, 45th, and 90th days.

It was found that the Pt/Ti_3C_2 sensor exhibits the higher response to H_2S gas and better recognition response at 10–50 ppb of H_2S gas. Note that a spike is observed in the response curves of the sensors. The use of the static gas distribution method requires a certain amount of time for H_2S gas to diffuse into the gas chamber, and when it first comes into contact with high concentrations of H_2S, the response of the sensor rapidly increases. As H_2S gradually disperses evenly, the sensor's response decreases and tends to stabilize. The process leads to the appearance of the spike. It can be concluded that both the Pt/Ti_3C_2 sensor and the Pt/C sensor exhibit a linear positive response to H_2S within the range of 0.01–200 ppm (Fig. 3c). The sensitivity of the Pt/Ti_3C_2 sensor (0.162 μA/ppm) is higher than that of the Pt/C sensor (0.112 μA/ppm). The baseline current of the sensor running in air for 1500 s was collected (Fig. 3d), and it can be seen that, compared to the Pt/C sensor, the current noise of the Pt/Ti_3C_2 sensor is relatively small. The lower the current fluctuation, the easier it is for the sensor to recognize H_2S. When the signal-to-noise ratio ($SNR = I_{signal}/I_{noise}$) is equal to 3, the lowest detected concentration is considered the lower detection limit of the sensor. According to Figs. 3b and d, the SNR of Pt/Ti_3C_2 sensor for detecting 10 ppb H_2S is calculated to be 3.31, and the SNR of Pt/C sensor for detecting 200 ppb H_2S is calculated to be 1.64. Meanwhile, the SMSI transfers electrons from Ti_3C_2 to Pt nanoparticles, thereby promoting catalytic oxidation of adsorbed gas molecules on the catalyst surface. Therefore, the Pt/Ti_3C_2 sensor has a lower detection limit of 10 ppb. In addition, the Ti_3C_2 sensor exhibits a response current of 2–3 nA for both 10 ppm and 50 ppm H_2S (Fig. S4 in Supporting information), indicating Ti_3C_2 without Pt loading has poor catalytic ability for H_2S. It can be concluded that Ti_3C_2 as a carrier enhances the stability of Pt loading and also enhances the ORR activity of Pt, rather than acting as a catalyst. To evaluate the H_2S sensing performance, Table S1 (Supporting information) lists the comparison between the Pt/Ti_3C_2 sensor and other H_2S sensors reported in recent years. It was found that the Pt/Ti_3C_2 sensor has a low detection limit, which can immediately detect H_2S concentration changes or H_2S leaks, and people can take relevant actions.

Repeatability and long-term stability are also important indicators for sensors. Fig. 4a shows the 10-cycle response/recovery curve of the Pt/Ti_3C_2 sensor at 10 ppm H_2S. Compared with the initial response value, the maximum fluctuation of subsequent response values is 4.4%, indicating excellent repeatability of the sensor. Fig.

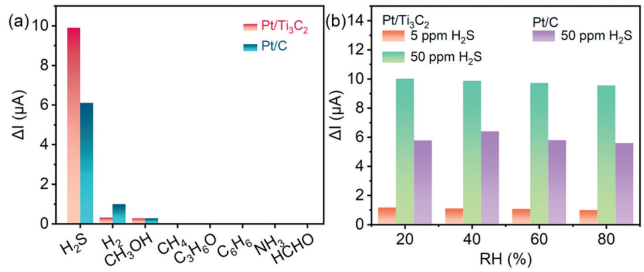

Fig. 5. (a) Comparison of selectivity between Pt/Ti_3C_2 and Pt/C sensors for different gases. (b) Changes in response values of Pt/Ti_3C_2 sensors and Pt/C sensors to H_2S at different humidity levels.

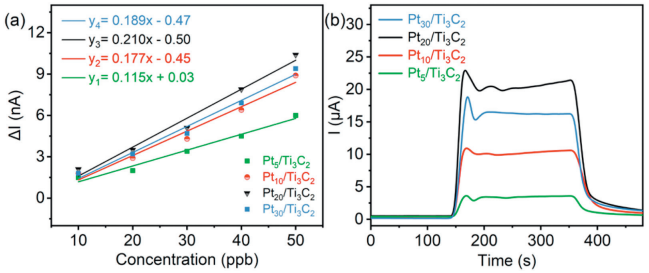

Fig. 6. Comparison of response values of four sensors to (a) 10-50 ppb H_2S and (b) 50 ppm H_2S.

4b shows that with each injection of 1 ppm H_2S, the current significantly increases, and the response current for each increase is almost the same, then remains stable after a certain time until the gas is pulled out and the current finally recovers. The above result indicates that the Pt/Ti_3C_2 sensor has good repeatability and can achieve continuous detection of H_2S. Fig. 4c shows the change in the response value of the sensor to 50 ppm H_2S over a period of 90 days, measured every 5 days. It can be seen that the response of the Pt/Ti_3C_2 sensor decreases by 2%, which is lower than that of the Pt/C sensor (22.9%), indicating that the Pt/Ti_3C_2 sensor has very good long-term stability. The response/recovery curves of the Pt/Ti_3C_2 sensor at 10^{th}, 45^{th}, and 90^{th} days are shown in Fig. 4d. This also indicates excellent long-term stability of the Pt/Ti_3C_2 sensor.

Other gas interference and relative humidity (RH) are also factors that affect the performance of gas sensors. Fig. 5a shows the responses of the Pt/Ti_3C_2 sensor and the Pt/C sensor to different gases with the same concentration (50 ppm), such as H_2, CH_3OH, H_2S, CH_4. Compared to the Pt/C sensor, the Pt/Ti_3C_2 sensor has a higher response to H_2S and a smaller response to other interfering gases. In addition, the response/recovery curves of the Pt/Ti_3C_2 sensor to H_2 and CH_3OH gases are also different from those of H_2S. So different gases can be distinguished by detecting their response characteristics. The above results indicate that the Pt/Ti_3C_2 sensor has good selectivity for H_2S gas. Fig. 5b shows the changes in response current values of the Pt/Ti_3C_2 sensor and the Pt/C sensor to H_2S at different relative humidity (20%, 40%, 60%, and 80% RH). As the relative humidity increases, the change in ΔI of the Pt/Ti_3C_2 sensor is within 5%, and the change in ΔI of the Pt/C sensor is within 10%. This indicates that the relative humidity has little impact on sensors, as the sealing structure and waterproof breathable film of the sensor prevent water vapor from entering the sensor.

The influence of Pt loading amount on sensor performance was investigated. Fig. 6 shows the performance of Pt_5/Ti_3C_2, Pt_{10}/Ti_3C_2, Pt_{20}/Ti_3C_2, and Pt_{30}/Ti_3C_2 sensors towards 10–50 ppm H_2S and 50 ppm H_2S. It was found that the sensitivity values of the Pt_5/Ti_3C_2, Pt_{10}/Ti_3C_2, Pt_{20}/Ti_3C_2, and Pt_{30}/Ti_3C_2 sensors exposed to low concentration H_2S are 0.115 nA/ppb, 0.177 nA/ppb, 0.21 nA/ppb, and 0.189 nA/ppb, respectively, and their response values to 50 ppm H_2S are 3.1 μA, 9.8 μA, 20.7 μA, and 16.1 μA, respectively. It is evident that as the loading content of Pt increases, the sensor's response to H_2S increases. This is attributed to the fact that as the loading content of Pt on the Ti_3C_2 surface increases, the number of active sites increases, leading to an increase in sensor response current. But when the Pt loading content increases to 30 wt%, Pt nanoparticles agglomerated (Fig. S6 in Supporting information), leading to a decrease in active sites and ultimately a decrease in sensor response current. This provides a certain reference for the application of sensors in different scenarios.

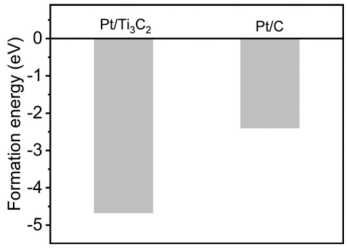

Fig. 7. Formation energy of Pt combined with Ti_3C_2 and C supports.

It has been known that the sensing mechanism of gas sensors depends on a series of redox reactions on the electrode surface. When H_2S reaches the surface of the working electrode, the H_2S molecule undergoes an oxidation reaction catalyzed by the catalyst material, producing hydrogen ions and releasing electrons. Hydrogen ions are transferred to the counter electrode through a proton membrane, while electrons are transferred to the counter electrode through an external circuit, where they undergo a reduction reaction with oxygen. The concentration of H_2S gas has a linear relationship with the generated current, so the concentration of H_2S can be determined by detecting the current of the sensor. The reactions that occur at the working electrode and counter electrode are as follows (Eqs. 1 and 2):

Reaction on the working electrode is:

$$H_2S \rightarrow S + 2H^+ + 2e^- \quad (1)$$

Reaction on the counter electrode is:

$$2H^+ + 1/2O_2 + 2e^- \rightarrow H_2O \quad (2)$$

DFT calculations were carried out to further explore the improved H_2S sensing mechanism of the modified Pt/Ti_3C_2. The influence of the carrier on H_2S detection was first investigated. Fig. 7 shows the formation energies of Pt/Ti_3C_2 and Pt/C. One can see that compared with Pt/C, Pt/Ti_3C_2 has a lower formation energy, indicating that the structure of Pt/Ti_3C_2 is more stable than that of Pt/C. Therefore, as an excellent carrier, Ti_3C_2 makes it difficult for Pt particles to detach from its surface during long-term operation, improving the sensor's long-term stability.

The H_2S sensing mechanism was also greatly affected by the terminal groups of Ti_3C_2. As reported, some terminal groups such as -F, -OH, -O and their combinations inevitably exist on the surface of MXene prepared by the etching method. XPS results show that before H_2 annealing treatment, Ti_3C_2 is terminated with -F/-OH groups. The calculation analysis demonstrates that when Pt nanoparticles are loaded on or near -OH groups, it will make it very easy for the H atom in -OH groups to transfer to the surface of Pt nanoparticles (Fig. S7 in Supporting information), affecting the catalytic activity of the Pt nanoparticles and reducing the stability of the material. When the material is subjected to H_2 annealing treatment, the surface is capped by -O/-OH groups and Pt nanoparticles are modified on the Ti_3C_2 surface *via* Pt-O-Ti bonding. Pt-

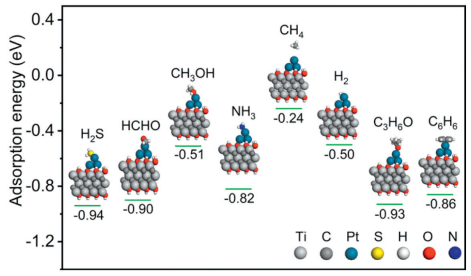

Fig. 8. The adsorption energy of various gas molecules on Pt/Ti_3C_2 surface.

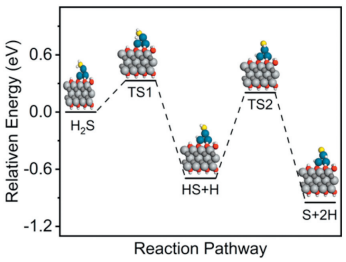

Fig. 9. The calculated energy profiles of different reaction routes of H_2S gas molecules on the surface of Pt/Ti_3C_2.

O-Ti bonding coexists stably with adjacent -OH terminal groups, suggesting the material is stable. As shown in Fig. S8 and Table S2 (Supporting information), it was found that when Pt occupies -O terminal groups, the bond length between its interface atoms is shorter than when Pt occupies -F terminal groups. The shorter bond length is beneficial for enhancing the interaction between the carrier and Pt and achieving a more stable structure. In addition, the formation energy of Pt/Ti_3C_2 with -F/-OH terminal groups (−1.56 eV) is higher than that of Pt/Ti_3C_2 with -O/-OH terminal groups (−4.67 eV), confirming the more stable Pt/Ti_3C_2 structure with -O/-OH terminal groups. Therefore, it has been proven that -O/-OH terminal groups instead of -F/-OH terminal groups enhance the interface interaction between Pt and Ti_3C_2 and ultimately prolong the sensor's service life.

The catalytic activity of loaded noble metals is key to achieving high-performance H_2S sensors. The adsorption and decomposition of H_2S on the Pt/Ti_3C_2 surface play an important role in the kinetic reaction process of H_2S sensing. As we all know, low adsorption energy can easily cause more gas molecules to adsorb on the surface of the working electrode and undergo the oxidation reaction, improving the response of the sensor to the gas molecules [45]. The adsorption energy for H_2S molecules on Pt/Ti_3C_2 and Ti_3C_2 was first investigated by DFT calculation, and the results are shown in Fig. S9 (Supporting information). It was found that Pt modification significantly decreases the adsorption energy of Pt/Ti_3C_2 compared with Ti_3C_2. The introduction of Pt can increase surface affinity to H_2S gas and provide more active sites in the reaction process, which is favorable to improving the sensitivity of the sensor. Furthermore, the adsorption energies of different gases on Pt/Ti_3C_2 were also studied by DFT calculation. As shown in Fig. 8, the adsorption energy of H_2S (−0.94 eV) is lower than that of other gases, revealing that H_2S is more easily adsorbed on the surface of the working electrode. This is one of the reasons why sensors have good selectivity for H_2S. Meanwhile, the kinetic decomposition reaction process of H_2S on the Pt/Ti_3C_2 surface was explored by DFT calculation as shown in Fig. 9. Pt modification facilitates the decomposition of absorbed H_2S gas into HS and H species after the very low energy barrier of 0.32 eV is overcome. After this reaction, HS species is still absorbed on the initial Pt atom, while H species moves to the nearest Pt atom. Afterwards, under the catalysis of Pt modification, the newly generated HS species continues to decompose into H and S species with a low energy barrier of 0.89 eV, where only newly formed H species moves to the second nearest Pt atom and other species continues to remain on the original Pt atom. The above results indicate that the catalytic activity of loaded noble metal accelerates the kinetic reaction process of H_2S sensing and realizes good sensitivity and high selectivity of the sensor.

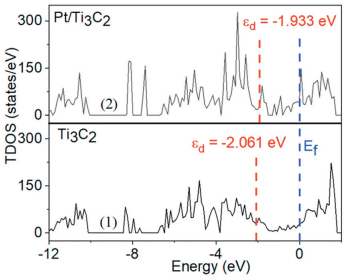

Fig. 10. Total density of state: (1) Ti_3C_2 and (2) Pt/Ti_3C_2.

In addition, we also calculated the total density of state (TDOS) of Ti_3C_2 before and after loading Pt nanoparticles (Fig. 10). It was found that the d-band center of the material before and after Pt loading changes from -2.061 eV to -1.933 eV. This indicates that there is an electron exchange interaction between Pt and Ti_3C_2, where electrons transfer to Pt atoms, causing the d-band center of Pt to shift downward, which is beneficial for improving the catalytic activity of the material. According to Bader's theory, it has also been proven that the number of electrons transferred from H_2S to Pt/Ti_3C_2 is about 0.14 |e|. The above results reveal that Pt catalyst is able to change the electronic structure of materials and help transfer effective charge.

In summary, we successfully designed and prepared stable Pt loaded Ti_3C_2 material with -O/-OH terminal groups and their corresponding fuel cell-type H_2S gas sensors. And the gas sensing experimental results reveal that the gas sensing performance is significantly improved with sensitivity up to 0.162 μA/ppm and a detection limit as low as 10 ppb compared to traditional Pt/C sensors. Specially, the sensor has good cyclic repeatability, long-term stability, and high selectivity. The DFT calculations and experimental results indicate that the Pt-O-Ti bonding formed between Pt and Ti_3C_2 reduces the formation energy of the material (−4.67 eV), thereby improving the stability of the sensor. At the same time, low H_2S adsorption energy (−0.94 eV) and low H_2S dissociation barrier (less than 0.89 eV) are also key factors for the sensor's good response to H_2S. In addition, the sensor has advantages such as no external voltage, zero-power consumption, and simple manufacturing process, which are expected to be applied in high-performance commercial sensors.

Declaration of competing interest

The authors declare that they have no known competing financial interests or personal relationships that could have appeared to influence the work reported in this paper.

CRediT authorship contribution statement

Huakang Zong: Writing – original draft, Methodology, Formal analysis, Data curation, Conceptualization. **Xinyue Li:** Methodology, Investigation, Formal analysis, Conceptualization. **Yanlin Zhang:** Writing – review & editing, Methodology, Formal analysis. **Faxun Wang:** Writing – review & editing, Resources. **Xingxing Yu:** Resources, Investigation. **Guotao Duan:** Writing – review & editing, Validation, Supervision, Project administration, Conceptualization.

Yuanyuan Luo: Writing – review & editing, Validation, Supervision, Software, Project administration, Funding acquisition.

Acknowledgments

The authors acknowledge the support from the National Key R&D Program of China (No. 2023YFB3210102). The authors are grateful for Analytical & Testing Center of Huazhong University of Science and Technology for the support in structure and morphology characterization.

Supplementary materials

Supplementary material associated with this article can be found, in the online version, at doi:10.1016/j.cclet.2024.110195.

References

[1] D. Bu, Y. Wang, N. Wu, Chin. Chem. Lett. 32 (2021) 1799–1802.
[2] S. Li, L. Xie, G. Luo, Chin. Chem. Lett. 33 (2022) 551–556.
[3] H.W. Thompson, Nature 127 (1931) 629-629.
[4] O. Yassine, O. Shekhah, A.H. Assen, Angew. Chem. Int. Ed. 55 (2016) 15879–15883.
[5] X. Sun, G. Jiang, P.L. Bond, J. Keller, Water Res. 157 (2019) 463–471.
[6] X. Zhang, J. Zhao, H. Wang, ACS Sens. 8 (2023) 4179–4188.
[7] D. Liu, Q. Wang, J. Wu, Y. Liu, Environ. Chem. Lett. 17 (2019) 259–276.
[8] A.Y. Mironenko, A.A. Sergeev, A.E. Nazirov, Sens. Actuators B: Chem. 225 (2016) 348–353.
[9] H. Moser, W. Poelz, J.P. Waclawek, J. Ofner, B. Lendl, Anal. Bioanal. Chem. 409 (2017) 729–739.
[10] T. Xu, J. Zhao, F. Zhao, W. Cong, G. Wang, Sens. Actuators B: Chem. 394 (2023) 134338.
[11] N. Zheng, X. Li, S. Yan, J. Mater. Chem. A 8 (2020) 2376–2386.
[12] H.M. Huang, H.Y. Li, X.X. Wang, X. Guo, Sens. Actuators B: Chem. 238 (2017) 16–23.
[13] C. Li, X. Qiao, J. Jian, Chem. Eng. J. 375 (2019) 121924.
[14] J. Zhao, H. He, J. Guo, ACS Sens. 8 (2023) 2824–2833.
[15] R. Kou, H. He, Y. Lu, Chem. Eng. J. 476 (2023) 146546.
[16] H. He, C. Zhao, J. Xu, ACS Sens. 6 (2021) 3387–3397.
[17] Y. Zhao, Y. Yang, L. Cui, F. Zheng, Q. Song, Biosens. Bioelectron. 117 (2018) 53–59.
[18] X. Yang, Y. Zhang, X. Hao, Sens. Actuators B: Chem. 273 (2018) 635–641.
[19] Q. Huang, W. Li, T. Wu, Electrochem. Commun. 88 (2018) 93–96.
[20] V. Paolucci, J. De Santis, V. Ricci, et al., ACS Sens. 7 (2022) 2058–2068.
[21] P. Ding, D. Xu, N. Dong, et al., Chin. Chem. Lett. 31 (2020) 2050–2054.
[22] G. Jiang, T. Cumberland, X. Fu, ACS Sens. 6 (2021) 752–763.
[23] W. Li, X. Yang, Y. Zhang, Sens. Actuators B: Chem. 311 (2020) 127900.
[24] C. Huang, J. Zhao, F. Qu, J. Wang, M. Yang, Sens. Actuators B: Chem. 346 (2021) 130516.
[25] C. Huang, D. Liu, D. Wang, J. Hazard. Mater. 423 (2022) 127193.
[26] M.Z. Ghavidel, M.R. Rahman, E.B. Easton, Sens. Actuators B: Chem. 273 (2018) 574–584.
[27] A. Modjtahedi, A. Amirfazli, S. Farhad, Sens. Actuators B: Chem. 234 (2016) 70–79.
[28] K. Hu, Y. Zhang, J. Zhu, Chin. Chem. Lett. 35 (2024) 109423.
[29] Z. Zhang, J. Liu, J. Gu, L. Su, L. Cheng, Energy Environ. Sci. 7 (2014) 2535–2558.
[30] Z. Wu, D. Dang, X. Tian, ACS Appl. Mater. Interfaces 11 (2019) 9117–9124.
[31] X.L. Tian, Y.Y. Xu, W.Y. Zhang, ACS Energy Lett. 2 (2017) 2035–2043.
[32] G. Fisseha, Y. Hu, Y. Yu, Chin. Chem. Lett. 35 (2024) 108445.
[33] Y. Lee, J.H. Ahn, H.-Y. Park, Nano Energy 79 (2021) 105363.
[34] Z. Kang, J. Cai, D. Ye, Chem. Eng. J. 446 (2022) 446P445.
[35] Y. Wang, J. Wang, G. Han, Ceram. Int. 45 (2019) 2411–2417.
[36] J. Jiang, S. Bai, J. Zou, Nano Res. 15 (2021) 6551–6567.
[37] X. Li, X. Ma, H. Zhang, Chem. Eng. J. 455 (2023) 140635.
[38] X.H. Xie, S.G. Chen, W. Ding, Y. Nie, Z.D. Wei, Chem. Commun. 49 (2013) 10112–10114.
[39] Z. Zhang, C. Liu, Y. Dai, ACS Appl. Energy Mater. 5 (2022) 14957–14965.
[40] C. Xu, C. Fan, X. Zhang, ACS Appl. Mater. Interfaces 12 (2020) 19539–19546.
[41] W. Zhao, B. Jin, L. Wang, Chin. Chem. Lett. 33 (2022) 557–561.
[42] K. Huang, Z. Li, J. Lin, G. Han, P. Huang, Chem. Soc. Rev. 47 (2018) 5109–5124.
[43] M. Lu, H. Li, W. Han, J. Energy Chem. 31 (2019) 148–153.
[44] Y. Lee, S.J. Kim, Y.J. Kim, J. Mater. Chem. A 8 (2020) 573–581.
[45] B. Song, D. Choi, Y. Xin, C.R. Bowers, H. Hagelin-Weaver, Angew. Chem. Int. Ed. 60 (2021) 4038–4042.